GRID GENERATION FROM VIDEO CAPTURE FOR MESHLESS METHOD THERMAL SIMULATIONS

Khaoula Lassoued [(a)], Tonino Sophy[(a)], Luis Le Moyne[(a)], Nesrine Zoghlami[(b)]

[(a)] DRIVE – ISAT EA 1859, 49, rue Mademoiselle Bourgeois, 58000 NEVERS, FRANCE.
[(b)] CONPRI – 99/UR/11-29, Rue Omar Ibn-Elkhattab, 6029 GABES, TUNISIA

[(a)] khaoulalassoued@gmail.com, [(b)] nesrine.zoghlami@gmail.com

ABSTRACT

A dynamic grid generation tool based on contour reconstruction and a Meshless Diffuse Approximation Method (DAM) is developed. The purpose is extracting the points cloud involved in the Meshless simulation from a digitalized picture or a video capture. Each frame taken from an ultra-speed camera video is transformed into a set of points.

After several image treatment investigations, a threshold-Hough association method is adopted and tested with circular and more complex shaped object.

The obtained grids are then used in numerical simulations with the Diffuse Approximation Meshless method. Transient heat diffusion and steady state convection are simulated. Results are presented as isotherms and streamlines.

The presented method seems to create DAM compatible grids as the isotherms are in respect with the conduction phenomenon and the streamlines fits to the references corresponding to similar cases.

Keywords: heat transfer, fluid flow, images and video processing, circular and complex shape object.

1. INTRODUCTION

Numerical simulation is widely used in advanced technology studies, especially in engineering field. Indeed, it is necessary to use adapted numerical method to produce convincing simulations of physical event such as fluid flow (smoke or water), thermal diffusion and natural or forced convection.

The choice of numerical methods to solve and represent the describing equations depends ideally on application fields.

In the past, to solve systems governed by Partial Differential Equations (PDEs), Finite Difference Method (FDM) Boutayeb (1991) and the Finite Element Method (FEM) Long (1995) which reduce the computational problem of complex geometries, were widely used. In spite of the great success of the so-called method as effective numerical tools for the solution of boundary values problems on complex domains, there has been, over the past decades, a growing interest in numerical methods which not requires finite element meshes. This class of method is known as "meshfree" or "particle" method. Indeed, the main advantage of the meshless methods is the needlessness of any predefined mesh or elements between the nodes. It just requires a grid of points for the discretization. So far, a number of methods have been proposed, the first one beeing the Smooth Particle Hydrodynamics (SPH) Monagahn (1992). For example, Ahmadi *et al.* (2010) used a Moving Least Square approximation method (MLS) to simulate steady-state heat conduction in heterogeneous materials.

Even if particle methods do not need meshing of the domain, the spatial discretization requires a set of points. This can be done by mathematical functions, grid extracting from mesh generation software or more recently by image processing.

Furthermore, in image processing scientific field, many works have been done concerning object detection or reconstruction. Main applications concern medical field, automotive comfort or security, face detection (Viola 2001, Li 2002 and Sochman 2004) or national defense department.

So, the focus of this paper is the association of image processing advance for the automation of static or dynamic grid construction from an image or video capture and simulation by a meshless method.

In this work, a Diffuse Approximation Method (DAM) based on a moving weighted least square approximation Sophy (2002) is developed to simulate heat diffusion around free falling ball and to simulate a thermal fluid flow around different objects. This method was first introduced by Nayroles *et al.* in the beginning of the 90s Nayroles (1991).

In this contribution, we start by providing a general description of DAM. We then present several methods of image processing used to generate the points' grid from the image or video capture. Then, heat conduction numerical results are presented in terms of isotherms or temperature field and some results of natural or forced convection around a circular or a more complex shaped object are respectively shown.

2. METHOD DESCRIPTION

2.1. Meshless Diffuse Approximation Method

Let $\varphi : R^n \to R$ be a scalar field whose values φ_j are known at the points x_j of a given set of n nodes in the

studied domain D ∈ R^n. The diffuse approximation gives estimates of φ and its derivates up to an order k at any point M(x,y) ∈ D. The order 2 Taylor expansion of φ at M gives:

$$\varphi_j = \varphi + \frac{\partial \varphi}{\partial x}(x_j - x) + \frac{\partial \varphi}{\partial y}(y_j - y) + \frac{\partial^2 \varphi}{2!\partial x^2}(x_j - x)^2 + \frac{\partial^2 \varphi}{\partial x \partial y}(x_j - x)(y_j - y) + \frac{\partial^2 \varphi}{2!\partial y^2}(y_j - y)^2$$

(1)

For reason of simplification, let assume the following notation:

$$(x_j - x) \leftrightarrow x_j \quad (y_j - y) \leftrightarrow y_j$$

With the minimization of the quadratic error one can obtain expressions of φ and its derivatives at any desirable nodal point:

$$\left\{ \begin{array}{c} \varphi \\ \frac{\partial \varphi}{\partial x} \\ \frac{\partial \varphi}{\partial y} \\ \frac{1}{2!} \frac{\partial^2 \varphi}{\partial x^2} \\ \frac{\partial^2 \varphi}{\partial x \partial y} \\ \frac{1}{2!} \frac{\partial^2 \varphi}{\partial y^2} \end{array} \right\} = \left[A^M \right]^{-1} \cdot \sum_{M_j \in v^M} \omega(M_j, M) \left\{ \begin{array}{c} 1 \\ x_j \\ y_j \\ x_j^2 \\ x_j y_j \\ y_j^2 \end{array} \right\} \cdot \varphi_j$$

(2)

where the matrix $\left[A^M \right]$ is:

$$\left[A^M \right] = \sum_{M_j \in v^M} \omega(M_j, M) \cdot \begin{bmatrix} 1 & x_j & y_j & x_j^2 & x_j \cdot y_j & y_j^2 \\ x_j & x_j^2 & x_j \cdot y_j & x_j^3 & x_j^2 \cdot y_j & x_j \cdot y_j^2 \\ y_j & x_j \cdot y_j & y_j^2 & x_j^2 \cdot y_j & x_j \cdot y_j^2 & y_j^3 \\ x_j^2 & x_j^3 & x_j^2 \cdot y_j & x_j^4 & x_j^3 \cdot y_j & x_j^2 \cdot y_j^2 \\ x_j \cdot y_j & x_j^2 \cdot y_j & x_j \cdot y_j^2 & x_j^3 \cdot y_j & x_j^2 \cdot y_j^2 & x_j \cdot y_j^3 \\ y_j^2 & x_j \cdot y_j^2 & y_j^3 & x_j^2 \cdot y_j^2 & x_j \cdot y_j^3 & y_j^4 \end{bmatrix}$$

(3)

and ω is a weight-function of compact support, equal to unity at this nodal point, decreasing when the distance to the node increases and equal to zero outside a surrounding zone (mentioned as v^M) near the calculation node. In our study, we chose the following Gaussian window:

$$\left\{ \begin{array}{l} \omega(X, X_j - X) = \exp\left[-3\ln(10) \cdot \left(\frac{|X_j - X|}{\sigma} \right)^2 \right] \\ \omega(X, X_j - X) = 0 \quad if\, ((X_j - X)^2 \geq \sigma^2) \end{array} \right.$$

(4)

where σ is the radius of the weight function support.
Thus, any Partial Derivative Equation can be written in terms of different φ_j. This requires information on the position of each point of the grid which describes the domain.

As the ultimate objective of this contribution is the association of DAM with an automatic procedure to obtain the set of points, a description of different stage of our image processing is given in next section.

2.2. Image processing
In this section we show different used methods for image treatment. A brief description will be given for these methods. Our code development is based on a C++ language using an Open source Computer Vision library (OpenCV). To achieve the grid generation, the captured image has to be smoothed by filtering operations. This is necessary for edge detection then pixel classification.

2.2.1. Image preprocessing
When an image is acquired by a camera or other imaging system, the vision system for which it is intended is often unable to use it directly. Good image smoothing should be able to deal with different types of noise. In this paper, two image smoothing filters are used. Figure 1 shows an example of original image and the results obtained with a Gaussian linear filter and a Median non-linear filter which is very effective in removing salt and pepper and impulse noise while retaining image details.
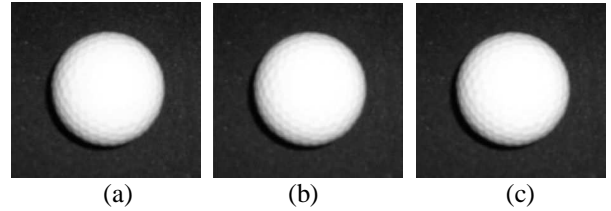

(a)   (b)   (c)

Figure 1: Smoothing filters, Original image (a), Gaussian filter (b) and Median filter (c).

2.2.2. Edge detection
As seen before DAM also needs the type of any point (if it is a point belonging to an edge, an object or a background point). It is then necessary to detect contours in the image. Edge detection is a fundamental tool used in most image processing applications to obtain information from the frames as a precursor step to feature extraction and object segmentation. This process not only detects boundaries between objects and the background in the image, but also the outlines within the object. To detect edges, many operators such as Sobel operator or Canny detector can be applied. The OpenCV library gives an important function that can detect contours. This function is called cvFindContours Bradski (2008). During our work many detection operators like Sobel or Canny, FindContour function and the Hough operator has been used (Figure 2 and 3).
- Sobel Operator:
It is a discrete differentiation operator, computing an approximation of the opposite of the gradient of the image intensity function.
- Canny Operator:

Canny's aim is to discover the optimal edge detection algorithm to satisfy good detection, good localization and minimal response

- cvFindContours:

The function cvFindContours retrieves contours from the binary image and returns the number of retrieved contours. The pointer "firstContour" is filled by the function. It will contain pointer to the first most outer contour or NULL if no contours is detected (if the image is completely black). Other contours may be reached from firstContour.
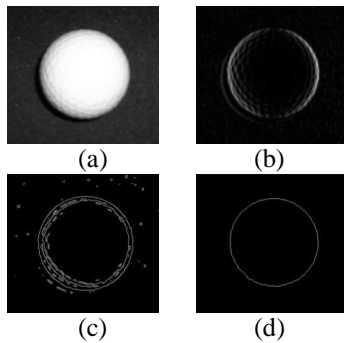

(a)   (b)

(c)   (d)

Figure 2: Edge detecting filters, Original image (a), Sobel detector (b), Canny detector (c), Find Contour (d)

- Hough transform:

The Hough transform is a feature extraction technique used in image analysis, computer vision and digital image processing Shapiro (2001). In our work, we used Hough to reconstruct the circles contours Kimme (1975). The Hough circle reconstruction technique highlights in the image the potential centers of r radius circles (figure 3-a). The center being detected, one can reconstruct the circle's contour (figure 3-b) or the entire object (figure 3-c).
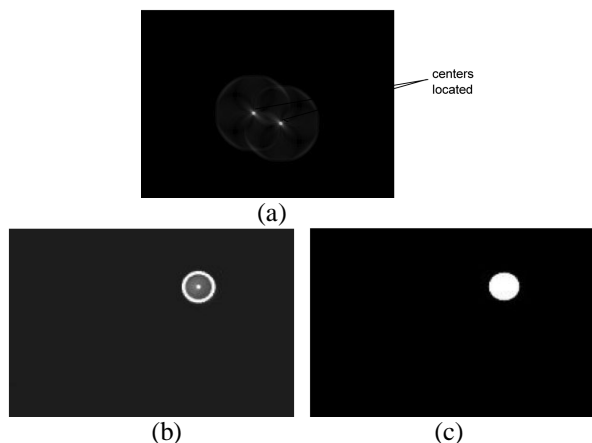

(a)

(b)   (c)

Figure 3 Hough circle transform, Center detection (a), (Ic) Contour image (b), (Io) Object image (c).

2.2.3. Acquisition

Two types of acquisition are made. Stand images are captured with a 640x480 resolution digital camera. No filters are used during the acquisition as the image is treated after. The video captures are made with a Photron FASTCAM Ultima APX-RS (Figure 4) high-

speed video camera that can reach 250 000 frames per second. During our work we capture 500 frames per second. This implies a dynamic system. Using Hough Transform (section 2.2.2) we treat this video frame per frame. Sometimes happen that the Hough detection is not suitable. This leads to the temporary disappearance of the object. A particular treatment is then applied. Our capture concerns a free falling ping pong ball. A black background is used to avoid additional treatment of the vicinity. High power spotlights are set at both sides of the scene to avoid a privileged light exposition side that can drive to spurious shadow (which can be interpreted as a contour). All this wariness is applied to reduce the future image processing time. Indeed, stand images are captured without black background and spotlights so the spurious contours are treated by the process.
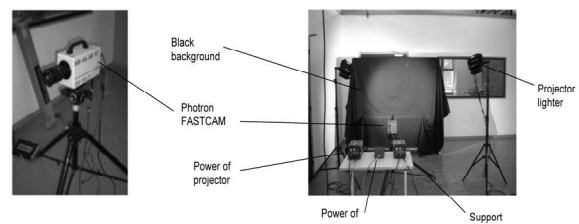

Figure 4: Photron FASTACAM Ultima APX-RS and material used.

An example of frame and the corresponding grid are shown in Figure 5. For the stand image, the picture is treated as one frame of the video.
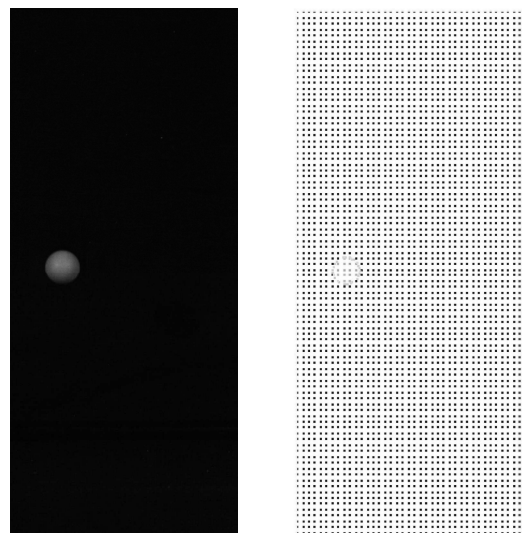

Figure 5: Grid point generated from frame

3. RESULTS

In this section some results of simulations obtained with DAM associated with the presented grid generation technique are shown. The first case concerns transient heat diffusion of a free falling circular object. The isotherms are presented for two different times and two different thermal conductivities. The second and the third cases, involve convective exchanges of a circular and a more complex shaped object. Streamlines and isotherms are calculated.

3.1. Heat diffusion

The dynamic grid is obtained with a video capture of a free falling rebounding ping-pong ball (Figure 5). The diffusion term of the transient heat equation (Eq 4) is discretized with the DAM and the transient term is approximated with a forward first order Finite Difference scheme:

$$-\frac{\rho C}{\lambda}\frac{\partial T}{\partial t}+\Delta T=0 \qquad (4)$$

where, ρ is the density, λ is the thermal conductivity, C is the specific heat capacity, T is the temperature and t is the time.

The boundary conditions are fixed temperatures on the limits of the domain ($T_c=0$) and the object ($T_h=1000$). All temperatures are initially set to $T_{init}=T_c$. The thermal conductivity values are $\lambda = 1$ W/mK and $\lambda = 8.10^{-3}$ W/mK while other physic properties are fixed to the value 1 SI. The time step Δt is fixed to 10^{-3}s.

The presented isotherms for times corresponding to 184 Δt (after the first rebound) and 404 Δt (during the second descent) (Figure 7) are in total accordance with the physical phenomenon. The increment of the thermal conductivity (Figure 8) intensifies the diffusive character of the problem and reduces the thermal inertia.
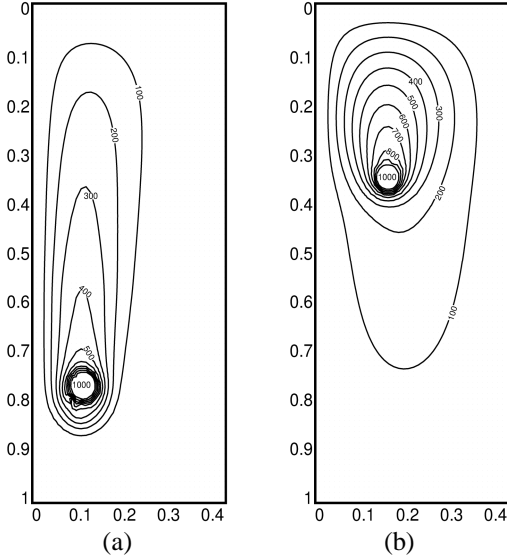
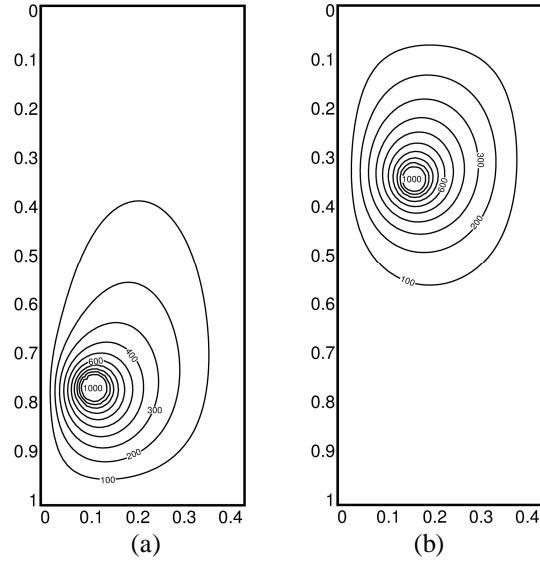Figure 7: Isotherms form for $\lambda =8\ 10^{-3}$, Ts=184Δt (a) and Ts=404Δt (b)

Figure 8: Isotherms form for $\lambda =1$, Ts=184Δt (a) and Ts=404Δt (b)

3.2. Flow over a circular shape object

In this case the steady state buoyancy flow around a circular shape object is simulated.

The governing equations are the Navier-Stokes equations in their dimensionless secondary variable form and the energy equation (Eq 5-7). As a pseudo-instationnary algorithm is used, the equations are in their transient form:

$$\frac{\partial^2 \Psi}{\partial x^2}+\frac{\partial^2 \Psi}{\partial y^2}=-\Omega \qquad (5)$$

$$\frac{\partial \Omega}{\partial t}+u\frac{\partial \Omega}{\partial x}+v\frac{\partial \Omega}{\partial y}=Pr\left(\frac{\partial^2 \Omega}{\partial x^2}+\frac{\partial^2 \Omega}{\partial y^2}\right)+Ra\,Pr\frac{\partial T}{\partial x} \qquad (6)$$

$$\frac{\partial T}{\partial t}+u\frac{\partial T}{\partial x}+v\frac{\partial T}{\partial y}=\nabla^2 T \qquad (7)$$

where Ψ represents the dimensionless stream function, Ω the vorticity, T the temperature, Ra the Rayleigh number and Pr the Prandtl number which are defined as:

$$Ra=\frac{g\,\beta\Delta T L_{ref}^3}{\nu\alpha}. \qquad (8)$$

$$Pr=\frac{\nu}{\alpha} \qquad (9)$$

whith g, β, ΔT, L_{ref}, ν and α being respectively the gravity, the thermal expansion coefficient, a characteristic temperature difference (T_h-T_c), a characteristic length (diameter of the circular object), cinematic viscosity and the thermal diffusivity.

The velocity component (u , v) are obtained with the stream function according to the equations:

$$u=\frac{\partial \Psi}{\partial y} \quad v=-\frac{\partial \Psi}{\partial x}. \qquad (10)$$

The fluid is assumed to be air (P=0.7). All the physical properties are constant except the density where the Boussinesq approximation is applied. The boundary conditions are fixed temperatures and stream functions

Proceedings of the International Conference on Modeling and Applied Simulation, 2012
978-88-97999-10-2; Affenzeller, Bruzzone, De Felice, Del Rio, Frydman, Massei, Merkuryev, Eds.

351

on the object (T_h, Ψ_{object}) and the walls (T_c, Ψ_{wall}). Non slip boundary conditions are applied (null velocities on the walls and the object).

Calculations are made for several Rayleigh number ranking from 1000 to 10^5. Figure 9 shows examples of streamlines obtained for Ra=1000 and Ra=10^5. Figure 10 shows temperature field for the same Ra numbers.
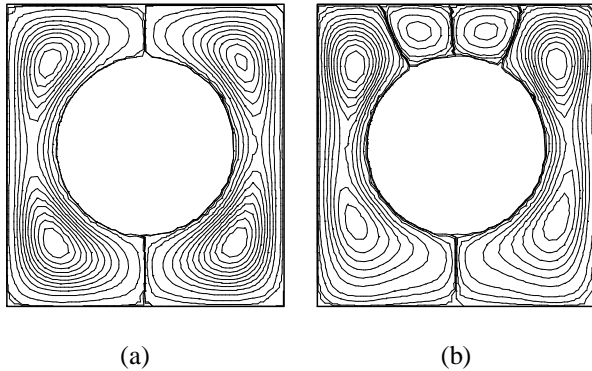

(a)   (b)

Figure 9: Streamlines for natural convection of Circular shaped object, Ra = 1000 (a) and Ra= 10^5 (b).

(a)   (b)
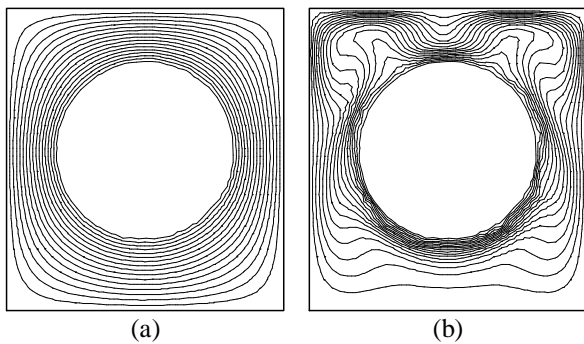
Figure 10: Isotherms for natural convection of Circular shaped object, Ra = 1000 (a) and Ra= 10^5 (b).

The results are in accordance with the references for similar problems as the structures of the flows respect the natural convection flows.

3.3. Flow over a car shape object

As a main advantage of meshless methods is the flexibility of the grid to deal with complex shapes, a car image is taken as original picture to built the grid. Nevertheless, the hardiness of the point cloud generation increases with the complexity of the involved shapes. The proposed method allows to generate complex grid from a picture (Figure 11). Then the DAM can be used to simulate convection exchanges on the obtained discretized domain.

For the natural convection the equations still the same as those used in section 3.2, with L_{ref} being the length (along the direction x) of the calculation domain.

For the forced convection the (Eq 6) and (Eq 7) respectively become:

$$\frac{\partial \Omega}{\partial t} + u\frac{\partial \Omega}{\partial x} + v\frac{\partial \Omega}{\partial y} = \frac{1}{Re}\left(\frac{\partial^2 \Omega}{\partial x^2} + \frac{\partial^2 \Omega}{\partial y^2}\right) \quad (11)$$

$$\frac{\partial T}{\partial t} + u\frac{\partial T}{\partial x} + v\frac{\partial T}{\partial y} = \frac{1}{Pr\,Re}\nabla^2 T \quad (12)$$

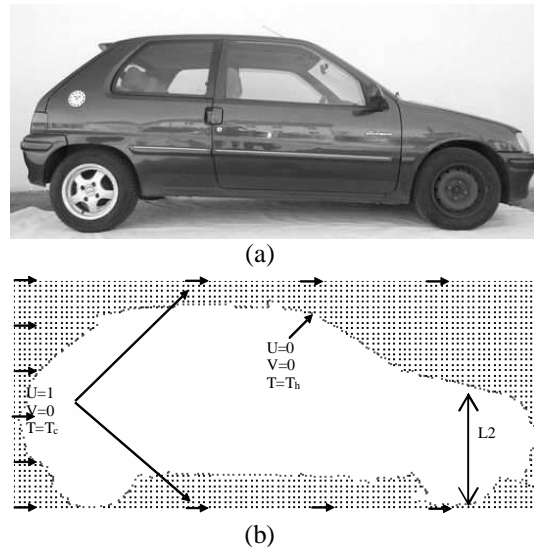and L_{ref} is fixed as the length L_2 shown in Figure 11b.

(a)

(b)

Figure 11: Complex shaped object (a), Automatic generated grid and Boundary Conditions (b)
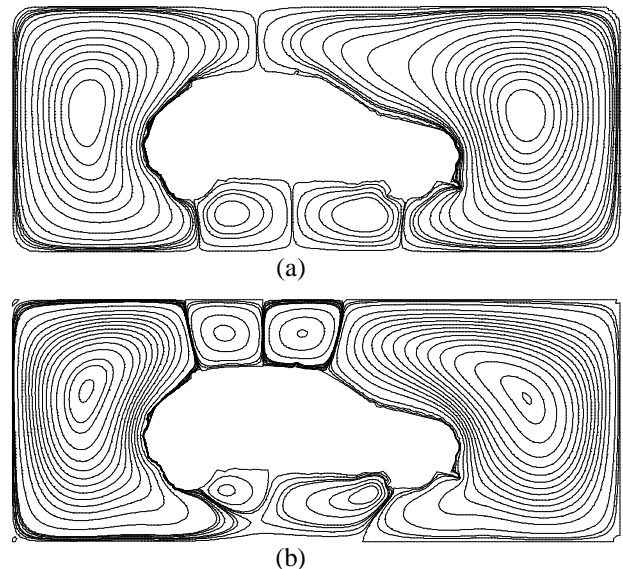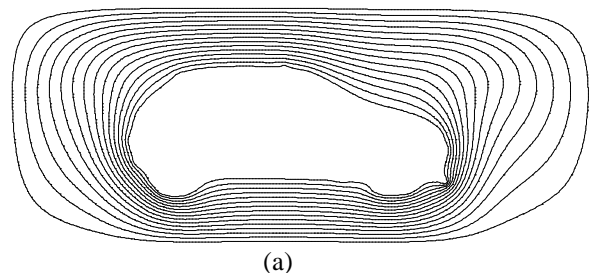

(a)

(b)

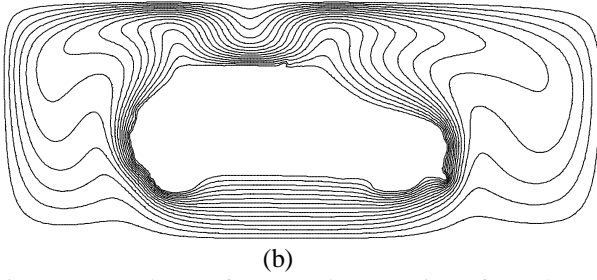Figure 12: Streamlines for natural convection of car shape object, Ra = 1000 (a) and Ra= 2.10^4 (b).

(a)

(b)

Figure 13: Isotherms for natural convection of car shape object, Ra = 1000 (a) and Ra= 2.10^4 (b).
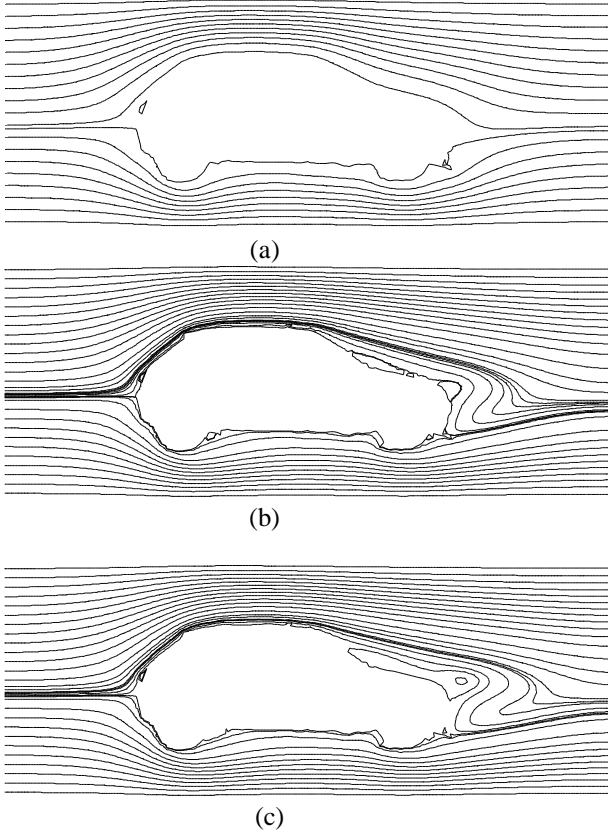

(a)

(b)

(c)

Figure 14: Streamlines for forced convection of car shape object, Re = 30 (a) Re=180 (b) and Re=210.
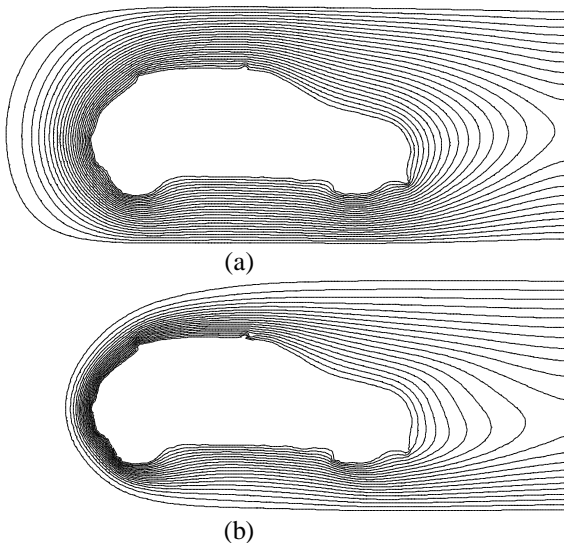

(a)

(b)

(c)

Figure 15: Isotherms for forced convection of car shape object, Re = 30 (a), Re= 180 (b) and Re=210 (c).

Streamlines and temperature fields are presented for natural and forced convection respectively on (Figure (12,13)) and (Figure (14,15)). Concerning natural convection, one can see that for low Rayleigh numbers (Figure (12a,13a) isotherms correspond to a diffusion regime and when Ra increases a plume flow appears. When simulating forced convection, a similar observation is made in respect of the Reynolds number. Simulations are made with Re=30, 180 and 270. Boundary conditions are in accordance with Figure 11b. The flow inlet is on the rear side of the car. This corresponds to a reverse car travelling simulation.

The ground is not taken into account so the flow can get around the tires. Indeed a 2D simulation can not simulate the flow within the car track. The simulation of the ground would lead to fluid accumulation near the tires.

For low Re numbers, streamlines are horizontal and incurve near the object. The increment of Re involves appearance of localized vortexes. These recirculations are representative of a flow detachment. They take place at the junction between the windshield and the hood, and between the hood and the headlights. The presence of these recirculations is probably relevant to the care brought to these locations in car conception. Figure 14c shows that another increment of Re leads to a merge of the eddies.

4. CONCLUSION

A meshless method grid generation procedure has been developed. It is the first image or video automatic grid generator associated to the Diffuse Approximation meshless Method. It seems to construct suitable grids either it concerns circular or more complex shaped object. The obtained point clouds have been tested with a Diffuse Approximation Method on transient heat diffusion or natural convection problems. Results are in agreement with the physical phenomena.

The obtained tool brings some facilities to the engineer or the searcher in terms of domain spatial discretization.

REFERENCES
Ahmadi, I., Sheikhy, N., Aghdam, M.M. and Nourazar, S.S., 2010. A new local meshless method for steady-state heat conduction in heterogeneous

materials. *Engeneering Analysis with Boundary Element*, 34, 1105_1112.

Boutayeb, A., Twizell, E.H., 1991. Finite-difference methods for twelfth-order boundary-value problems. *Journal of Computational and Applied Mathematics*, 35, 133_138.

Bradski, G.R., Kaebler, A., 2008. Learning OpenCV,Computer Vision with *OpenCV Computer Vision with the OpenCV Libarary*, O'Reilly Media, 234-244.

Kimme, C., Ballard, D. H., Sklansky, J., 1975. Finding circles by an array of accumulators. *Communications of the Association for Computing Machinery*, 18, 120_122.

Li, S., Zhu L., Zhang, Z.Q., Blake A., Zhang, H.J. and Shum, H., 2002. Statistical learning of multi-view face detection. *Proceedings of the 7th European Conference on Computer Vision*, May 2002 Copenhagen, Denmark.

Long, P., Jinliang, W. and Qiding, Z., 1995. Methods with high accuracy for finite element probability computing. *Journal of Computational and Applied Mathematics*, 59, 181_189.

Monaghan, J.J., 1992. Smooth particle hydrodynamics. *Annual. Reviews Astronomy and Astrophysics*, 30, 543-74.

Nayroles, B., Touzot, G., Villon, P., 1991. L'approximation diffuse, *Comptes Rendus de l'Académie des Sciences Paris*, 313, 133_138 Série II.

Shapiro, L. and Stockman, G., 2001. *Computer Vision. 1st ed*. New Jersey (USA):Prentice-Hall.

Sochman, J. and Matas, J., 2004. AdaBoost with totally corrective updates for fast face detection, *Proceedings of the 6th IEEE International Conference on Automatic Face and Gesture Recognition*, pp.445-450.

Sophy, T., Sadat, H., Prax, C., 2002. A meshless formulation for three dimensional laminar natural convection. *Numerical. Heat Transfer part B: Fundamental*, 41, 433_445.

Viola, P. and Jones, M., 2001. Rapid object detection using a boosted cascade of simple features, *Proceedings of the IEEE Computer Society Conference on Computer Vision and Pattern Recognition (CVPR 01)*, pp.511-518.